Gas adsorption and separation in realistic and idealized frameworks of organic pillared graphene: a comparative study †

Giovanni Garberoglio,*,‡,¶ Nicola M. Pugno,§,‖,⊥ and Simone Taioli‡,¶

‡*European Centre for Theoretical Studies in Nuclear Physics and Related Areas (ECT*) Bruno Kessler Foundation, Trento, Italy.*

¶*Trento Institute for Fundamental Physics and Applications (INFN-TIFPA), Trento, Italy.*

§*Laboratory of Bio-Inspired & Graphene Nanomechanics, Department of Civil, Environmental, and Mechanical Engineering, University of Trento, Trento, Italy.*

‖*Center for Materials and Microsystems, Fondazione Bruno Kessler, Trento, Italy.*

⊥*School of Engineering and Materials Science, Queen Mary University of London, London, United Kingdom.*

E-mail: garberoglio@fbk.eu

Abstract

In this work we present a systematic and thorough comparison between gas adsorption and energy storage properties in idealized or realistic models of organic-pillared reduced-graphene-oxide sheets.

Firstly, atomistic simulations, based on density functional theory, are used to generate the structures of these novel systems. Secondly, Grand Canonical Monte Carlo is

†This document is the unedited Author's version of a Submitted Work that was subsequently accepted for publication in *The Journal of Physical Chemistry C* copyright© American Chemical Society after peer review. To access the final edited and published work see http://dx.doi.org/10.1021/jp511953p

used to predict the adsorption properties of the proposed frameworks for two different gases, notably hydrogen and carbon dioxide.

While one can safely conclude that gas adsorption is strongly affected by the density of the pillars and the chemical composition of the compounds, a comparison between realistic idealized structures shows that even the corrugation of graphene sheets has a deep impact on such properties.

Finally, we produce evidence of the potentiality of these pillared structures to be used as gas separation devices by investigating the sieving of CO_2/H_2 mixture at room temperature.

Introduction

In recent years, there has been ever growing interest in technological applications of graphene-based compounds, with numerous groups succeeding in harnessing the peculiar characteristics of this material.

One of the most notable use of graphene is to produce carbon-based devices by exploiting its unsurpassed electronic properties.[1–5] In this respect, the interaction of small molecules with graphene has been studied in detail for tuning its electronic and optical properties, with particular emphasis to hydrogen.[6,7]

However, due to the large available area, the study of graphene hydrogenation and physisorption[8–10] may be interesting also as a prototype of hydrogen storage in carbon materials.[11]

To develop graphene-based nanostructures for storage purposes, it is convenient to start from the oxidized form of graphene, which is soluble as well as having better reactivity than CVD-graphene.[12] In this respect, graphene-oxide (GO) based membranes have been shown to have very interesting properties for fluid treatment, such as an exceptional selectivity for water,[13] and a promising chemisorption[14] or physisorption[15] capacity for hydrogen storage.

In order to exploit extensively these unique properties for fluid treatment, GO needs to be

arranged in a three-dimensional framework from its inherently bidimensional structure. One promising route is to insert spacers between GO layers. This procedure leads to a series of materials generally known as Pillared Graphene-Oxide Frameworks (PGOF). To the best of our knowledge the first attempts in this direction were made by Burress and coworkers,[16,17] using boron-containing compounds as spacers. Recently, Kumar and coworkers showed how to synthesize PGOF using organic linkers only.[18] The possibility of varying the type of linker and their density paves the way to the rational development of PGOFs with tailored properties.[19] Gas adsorption properties were experimentally characterized and found to be comparable with that of other nanoporous materials, such as Metal-Organic Frameworks (MOF).[20] Recently, various groups have been using a systematic approach to screen large classes of possible MOFs using computer simulations, with the aim of identifying those more suited to gas storage applications.[21–23] In these investigations, the availability of accurate and transferable description for the adsorbate–adsorbent interaction has been proven crucial.

Computer modeling of gas adsorption in MOFs is essential to gain microscopic insights on the mechanisms of adsorption (and/or diffusion) and enable a precise characterization of adsorption sites. This computational analysis provides important clues regarding the optimization of the properties for specific tasks.[24–26]

However, no systematic modeling approach to PGOF has been reported to date. The principal reason for this lack is that computational investigations are made cumbersome by the non-periodicity of the atomic structure of the reduced-GO-based (rGO) materials. Burress *et al.* performed simulations using idealized models of PGOFs, in order to assess the effect of pillar density on the amount of hydrogen adsorbed.[16] In particular, the graphene-oxide sheets were approximated with planar graphene sheets. A similar approach was adopted by Nicolaï and coworkers in their numerical investigation of water diffusion in PGOFs.[27,28]

Remarkably, no systematic assessment of the quality of these assumptions has been performed to date. The goal of this work is thus to gain real insights on the hydrogen adsorption

properties of PGOFs by comparing the results of idealized, as previously done, and realistic models. The same analysis will be repeated for a different gas, notably carbon dioxide. Furthermore the gas separation properties of the CO_2/H_2 mixture in this structure will be investigated.

In the first part of the paper we describe our quantum chemical approach leading to the generation of realistic PGOF structures with atomic-level detail. Our efforts have been inspired by the recent fully-organic PGOFs synthesized by Kumar *et al.*,[18] for which no computational model has been developed so far. In the second part of the paper, we present our results on the adsorption of hydrogen and carbon dioxide in PGOFs, comparing the results with idealized models. Finally, gas separation for the CO_2/H_2 mixture is discussed.

Modeling pillared graphene-oxide frameworks and gas adsorption therein

Structure generation

Reduced graphene-oxide is mostly obtained by oxidation of a pristine graphene sheet using a mixture of sulfuric acid, sodium nitrate and potassium permanganate, following a class of methods proposed by Hummers and Offeman.[29,30] In this process, oxygen reacts in an uncontrolled manner, thus creating a highly defective and amorphous material. In general, the interaction of oxygen with graphene results in dangling hydroxyl (OH) groups, or in epoxide functional groups (oxygen atoms bridging two C atoms of the graphene sheets).[31,32] In this process, some carbon atoms are removed, leaving defects on the surface.[12] Reduced graphene-oxide is generally characterized by a different percentage of oxygen atoms present in the final product, typically ranging from 8% to 25% in number.[30]

With the further goal of studying the respective adsorption and separation properties, we generated 4 different structures using atomistic simulations based on classical molecu-

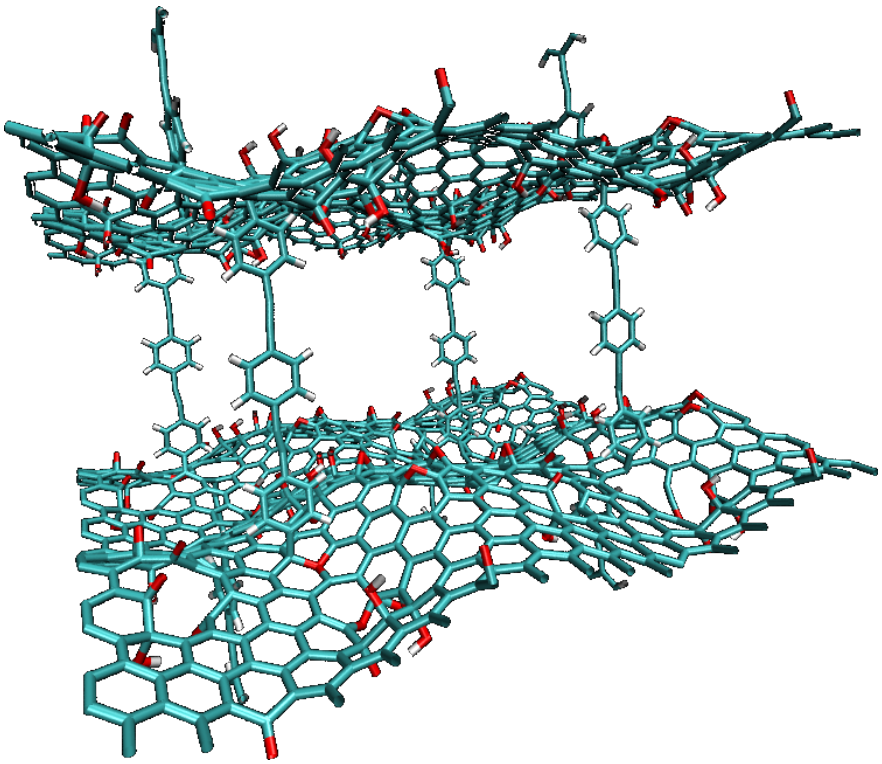

Figure 1: The PGO structure considered in this paper. Carbon, oxygen, and hydrogen atoms are colored in green, red, and white, respectively.

lar mechanics (MM), density functional theory (DFT) and its tight-binding approximation (DFTB). This latter approach has been shown to be a very good compromise between accuracy and speed in the calculation of many properties of MOFs.[33–37]

In order to generate a chemically meaningful PGO model structure, we started from a pristine graphene layer, using the program Avogadro[38] to substitute some randomly chosen carbon atoms with oxygen, making them either bridging oxygen atoms or protruding hydroxyl groups. The number of substituted oxygen atoms was chosen in order to have a coverage of 10% to 15% of the final graphene-oxide layer.[18] These rGO structures have been optimized using the MMFF94 force field.[39] The resulting structures have been further optimized using the DFTB+ program, implementing an efficient tight-binding approximation to DFT.[40] This step is necessary to describe the formation and disruption of bonds in the oxygen-rich carbon systems.

We used 0.5 fs timestep and a Nosé–Hoover thermostat sampling a NVT ensemble. The

target temperature of the thermostat was set to 1500 K for 100 ps and reached by specifying a temperature profile as follows. Temperature was linearly increased from 10 to 1500 K in 400 fs after an initial equilibration of 150 fs at a constant temperature of 10 K. The annealing, at the target temperature, was kept for 100 ps until structural equilibration. Byproducts, mainly consisting of CO molecules, obtained during these annealing periods were deleted. Finally, temperature was exponentially decreased to 10 K in 150 fs.

The rGO structures obtained were further relaxed by using DFT as implemented in the total-energy and molecular dynamics VASP code,[41] with an implementation of an efficient extrapolation for the electronic charge density.[42] The ion-electron interaction has been described using the Projector Augmented Wave (PAW) technique with single-particle orbitals expanded in plane waves with a cutoff of 400 eV. The Perdew–Burke–Ernzerhof (PBE) exchange-correlation potential[43] has been used to treat the electron-electron Coulomb interaction. In all DFT relaxation simulations, electronic and ionic temperature was fixed at 300 K with a corresponding Fermi smearing of the electronic density. Brillouin zone was sampled at the Γ point only. The rGO structures optimized via DFT were included in a supercell of 22×21 Å^2 in the lateral dimension and 20 Å in the direction orthogonal to the graphene sheet to avoid spurious interactions among periodic images. After DFT relaxation a 2×2 supercell in lateral dimension was created by periodically repeating the DFT supercell and reoptimized using DFTB. DFTB optimizations were performed using the Self-Consistent Charge approach, using the `matsci` parametrization for the Slater–Koster tables.[44] Even in this case we sampled the Brillouin zone at the Γ point only. Finally, four organic linkers and a second different 2×2 (obtained as previously) rGO sheet on the top of them were added to generate the three-dimensional superstructure reported in Fig. 1.

The first set of four linkers were added by creating chemically reactive sites (e.g., by removing a C atom) on a previously optimized rGO sheet already presenting crests and troughs. Pillars were rooted at the position of the chemically active sites. In this way, we favored the formation of covalent bonds with the linkers. This procedure has been repeated

again for an independently generated and optimized second layer. We carefully placed the pillars so to assure that a periodic bilayer structure was generated. The geometry so obtained was finally relaxed using DFTB.

Since the density of linkers in the materials synthesized in Ref. 18 was not specified, we used 4 linkers, with a final density of 0.2 linkers/nm^2. We report the principal characteristics of the four structures in Table 1.

The most striking feature of the realistic PGOF model is the fact that the rGO sheets are considerably buckled, with the appearance of clear crests and troughs. This peculiarity of the actual systems is completely neglected in the idealized modeling used so far in the literature and, as we will show below, does have a considerable impact on the prediction of the amount of gas adsorbed in these structures.

Table 1: Principal characteristics of the PGOFs modeled in this work. The "Flat model" is an idealized model of PGOF-1. The free volume is defined in Eq. (1).

Name	Oxygen %	Volume (Å^3)	Free volume (Å^3)	Mass (a.m.u.)
PGOF-1	10	72442	54470	21811
Flat model	10	80998	64571	20970
PGOF-2	10	87965	69692	22419
PGOF-3	15	76137	57613	22633
PGOF-4	15	91661	72415	23270

Simulation of gas adsorption

In this work, we performed as a first test case computer simulation of gas adsorption, notably hydrogen and carbon dioxide, in the optimized structures described in the previous section using standards force fields to model the adsorbate–adsorbent interaction. Molecular hydrogen is representative of those molecules having mainly van der Waals interactions with the adsorbent. In general, it turns out that molecular hydrogen can be effectively modeled as being a single Lennard-Jones center of force, with parameters given by $\varepsilon/k_{\mathrm{B}} = 34.2$ K and $\sigma = 3.18$ Å.[45]

In contrast, carbon dioxide is characterized by a quite significant electric quadrupole

moment, and electrostatic interactions have generally to be included in any successful model. We decided to use the EPM2 parametrization for the CO_2 molecule, which is made by Lennard-Jones centers and partial charges.[46]

The framework atoms have also been described as Lennard-Jones centers. Two force fields are being generally used in this case, either DREIDING[47] or the Universal Force Field;[48] since it turns out that the former generally performs slightly better than the second,[26,49,50] we decided to use it in our calculations, adopting the Lorentz–Berthelot mixing rules to calculate the interaction between unlike atoms. When simulating carbon dioxide, we considered also electrostatic effects by adding the electrostatic potential produced by partial charges on the framework atoms. These partial charges were calculated through a Mulliken population analysis from the DFTB calculations.

Adsorption simulations were performed using standard Grand Canonical Monte Carlo (GCMC) techniques. The chemical potential was related to the pressure of the reservoir gas using the van der Waals equation of state, whose parameters have been set to reproduce the position of the adsorbate critical point. For each external pressure we performed 1 million equilibration steps (one step being either an insertion, a deletion, or translation/rotation of an already adsorbed molecule), followed by 5 million production steps. One step every thousand was saved for off-line analysis.

When simulating hydrogen adsorption at cryogenic temperatures ($T = 77$ K) quantum diffraction are not negligible.[49] In principle, the path-integral formulation of quantum mechanics[51] would enable one to describe quantum effects in an accurate manner.[52–54] Nevertheless, the centroid approximation to the path integral[55] was shown to be remarkably accurate at this temperature, and thus has been adopted in this work. This approximation, that can be derived from quantum statistical mechanics, describes a quantum particle of mass m in thermal equilibrium as having a Gaussian distribution with variance given by $\sigma^2 = \beta\hbar^2/(12m)$.

In particular, the following analysis will be focused on the calculation of the excess

amount, N_{ex}, for a given adsorbate species. In detail, N_{ex} can be obtained by estimating the number density $\rho(T, P)$ of the adsorbate at the given thermodynamic condition (which we calculate using the van der Waals equation of state), and the available free volume for adsorption, V_{free}. V_{free} is conventionally defined as the volume of the region where the solid-fluid interaction between the framework and a Helium atom divided by the Boltzmann constant k_{B} is less than 10^4 K. This pore volume definition agrees with experimental measurements of adsorption, requiring the helium dead space for volumetric measurements and the buoyancy of the solid in helium for gravimetric measurements.[56]

In this paper, we modeled the He atom as a Lennard-Jones center with $\varepsilon/k_{\text{B}} = 10.22$ K and $\sigma = 2.556$ Å.

Finally, the number of adsorbed molecules is given by

$$N_{\text{ex}} = N - \rho(T, P)V_{\text{free}} \tag{1}$$

where N is the total number of gas molecules.

Results and discussion

Adsorption of Hydrogen

The adsorption isotherms for molecular hydrogen at $T = 77$ K are shown in Figure 2 for the four PGOFs considered in this work. In the range of pressures covered in our investigation, we do not see any tendency of the isotherms to show a saturation behavior. In fact, inspection of the computer-generated configurations shows that at $P = 10$ bar hydrogen accumulates on the GO sheets, with only a small amount to be found in the space within the sheets or in contact with the pillars.

We notice that at low pressures, all the PGOFs present a quite similar behavior. In fact, in this regime the isosteric heat of adsorption is roughly 5.7 kJ mol^{-1}, irrespectively of the

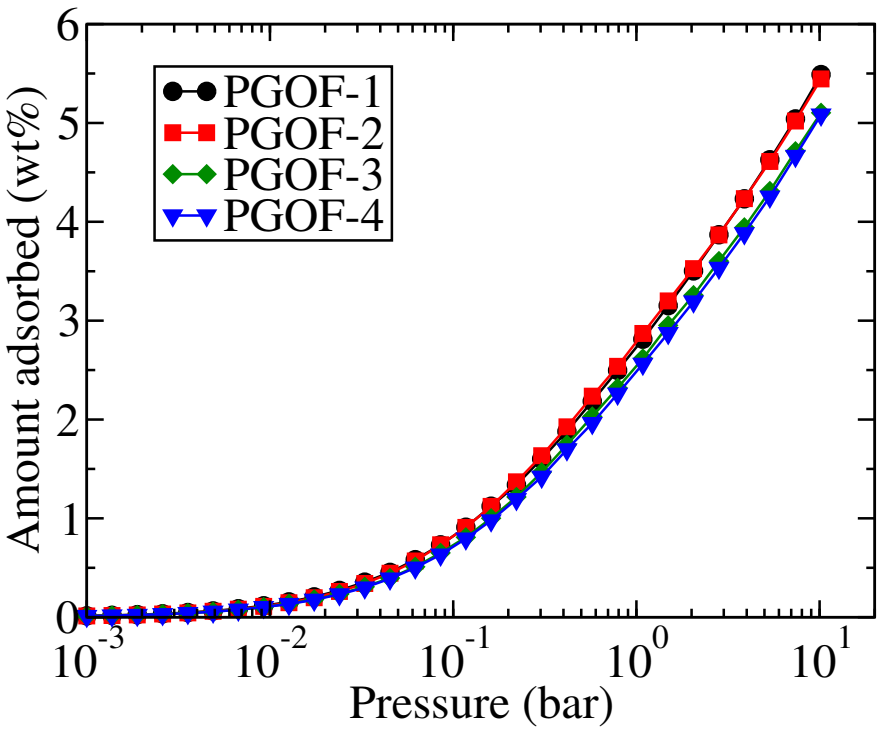

Figure 2: Isotherms of hydrogen adsorption at $T = 77$ K in the PGOFs modeled in this work.

framework investigated.

It is only at high pressure that the differences between the frameworks becomes apparent: the frameworks PGOF-1 and PGOF-2, with less content of oxygen than PGOF-3 and PGOF-4, adsorb more hydrogen than the other two.

The amount of hydrogen adsorbed in PGOFs at $T = 77$ K is comparable with the amount that is observed, both with experiments and computer simulations, in many MOFs[26] and Covalent Organic Frameworks.[57] However, the experimental results reported in Ref. 18 seem to indicate a that PGOFs should adsorb a significantly smaller amount, roughly by a factor of three at $P = 10$ bar. Unfortunately, a direct comparison between our calculations and the data reported in Ref. 18 is difficult to make, mostly because Kumar *et al.* do not estimate the density of linkers nor the percentage of oxygen in their samples. Our results are quite close to the one reported by Burress and coworkers in a similar material.[16] We also notice that Burress and coworkers study the amount of hydrogen adsorbed as a function of the linker

density, finding a significant variation. Thus one can argue that a linker density larger than ours in the samples investigated in Ref. 18 could safely explain the discrepancies observed.

Adsorption of Carbon dioxide

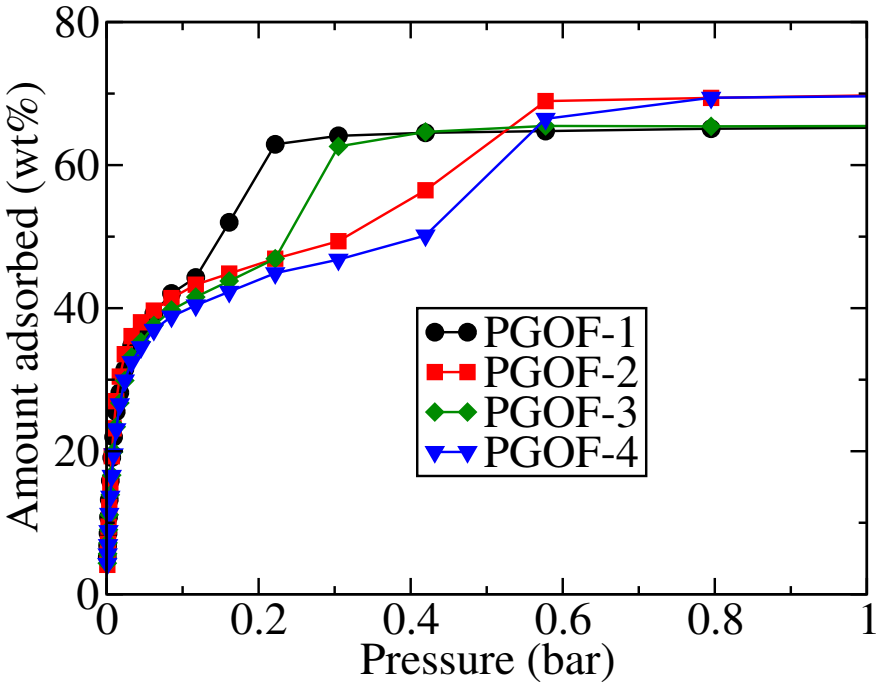

Figure 3: Isotherms of CO_2 adsorption at $T = 195$ K in the PGOFs modeled in this work.

The adsorption isotherms of carbon dioxide at $T = 195$ K are shown in Fig. 3 for the four PGOFs considered in this work. These isotherms have a qualitatively different shape than the hydrogen adsorption isotherms, displaying a pronounced step. The presence of this step is commonly observed in computer simulations of CO_2 adsorption (roughly at the same pressure and temperature than in our case), and is due to the fact that beyond a certain density of adsorbed molecules, the relatively strong quadrupolar electrostatic interaction between the CO_2 molecules further enhances the adsorption, creating the step in the isotherm.[58]

The pressure where the step is observed differs for all the PGOFs investigated here. This suggests that its position depends on both the oxygen density and the kind of pillar. Experimental data reported in Ref. 18 do not show the presence of a stepped behavior in

the same range of pressure analyzed here. As already discussed in the case of H_2 adsorption, this difference might be attributed to a different density of pillars and/or a different oxygen composition between our models and the actual samples. Nevertheless, we point out that, differently to what has been observed in the case of hydrogen adsorption, the amount of CO_2 adsorbed in our simulations (~ 60 wt%) is comparable with the experimental results.

Comparison with an idealized model

In a previous work,[11] Tozzini and Pellegrini showed that the corrugation of graphene sheets can strongly influence the hydrogen chemisorption. In order to check the possible effects of corrugation in our case (physisorption), we generated an idealized model of PGOF-1 by considering two ideal graphene sheets separated by a distance appropriate to contain the same linker as the PGOF-1 structure. On the two graphene sheets, 10% of the carbon atoms (chosen randomly) were substituted with oxygen atoms. We emphasize that this idealized model is only an approximation to the realistic one described above. In particular, the atomic positions and the topology of the system are not equal, although they are comparable. On each oxygen atom, we placed a partial charge equal to the average value of the oxygen partial charges in the DFTB+ calculations, $q_O = -0.36|e|$, where e is the electron charge. In order to assure charge neutrality, we placed a compensating charge $q_C = 0.12|e|$ on the three neighbors of the oxygen atoms. Given the random distribution of the oxygen centers within the graphene sheet, this procedure was not enough to assure charge neutrality, because it might happen that two oxygen were nearest neighbors. In this case, the oxygen charge was left untouched, and the remaining compensating charge distributed equally among the carbon atoms near the oxygen atoms. The geometrical parameters of the resulting structure are reported in Table 1.

Computer simulation of hydrogen and oxygen adsorption were performed in the same way as with the other PGOFs. The adsorption isotherms of H_2 at $T = 77$ K and of CO_2 at $T = 195$ K, are reported in Figures 4 and 5, respectively.

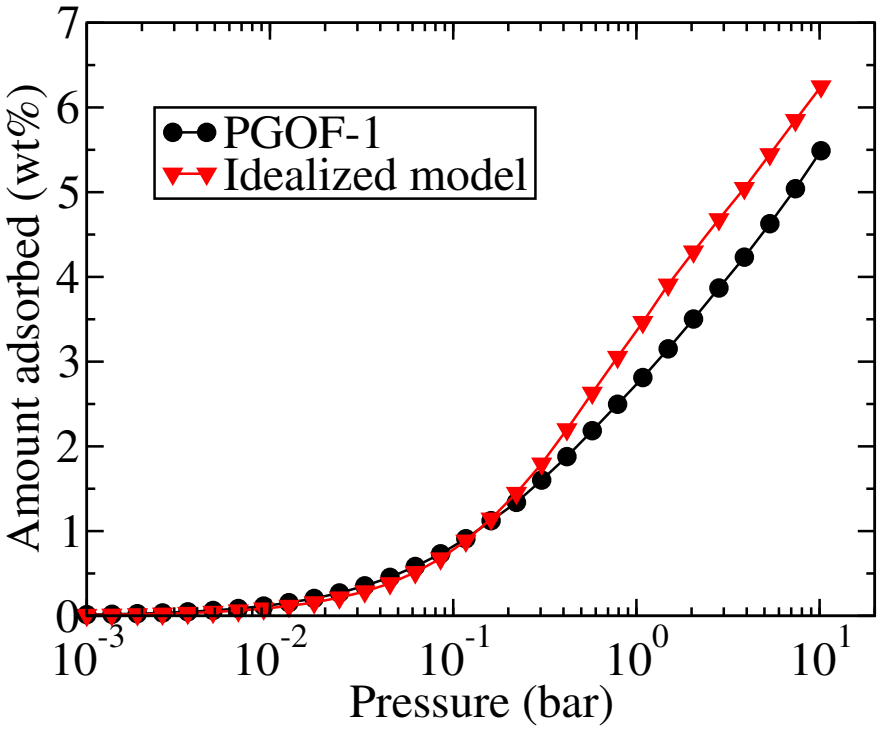

Figure 4: Adsorption isotherm of H_2 at $T = 77$ K in PGOF-1 (circles) and in the idealized model (triangle).

Two features are strikingly evident by analyzing these curves. The first is the slight tendency of the realistic model to adsorb more gas at low pressure (that is, low coverage regime). In this regime, the amount adsorbed is indeed determined by the solid-fluid potential energy surface. This tendency could be thus easily explained by the presence of troughs in the buckled graphene sheets of the realistic model, providing adsorption sites with a slightly higher interaction energy with the adsorbate, due to the favorable superposition of the attractive wells of the Lennard-Jones potential.

In the case of hydrogen, we observe a minimum energy of the idealized structure (indicated as idealized model in Fig. 4) equal to $V_{\rm flat}/k_{\rm B} = -871$ K, to be compared with the minimum energy for the interaction with PGOF-1 which is $V_{\rm PGOF-1}/k_{\rm B} = -1057$ K. However, this favorable energetics is contrasted by the relatively small region where the the solid-fluid potential attains its minimum, resulting in a modest increase of the amount adsorbed due to the effect of curvature.

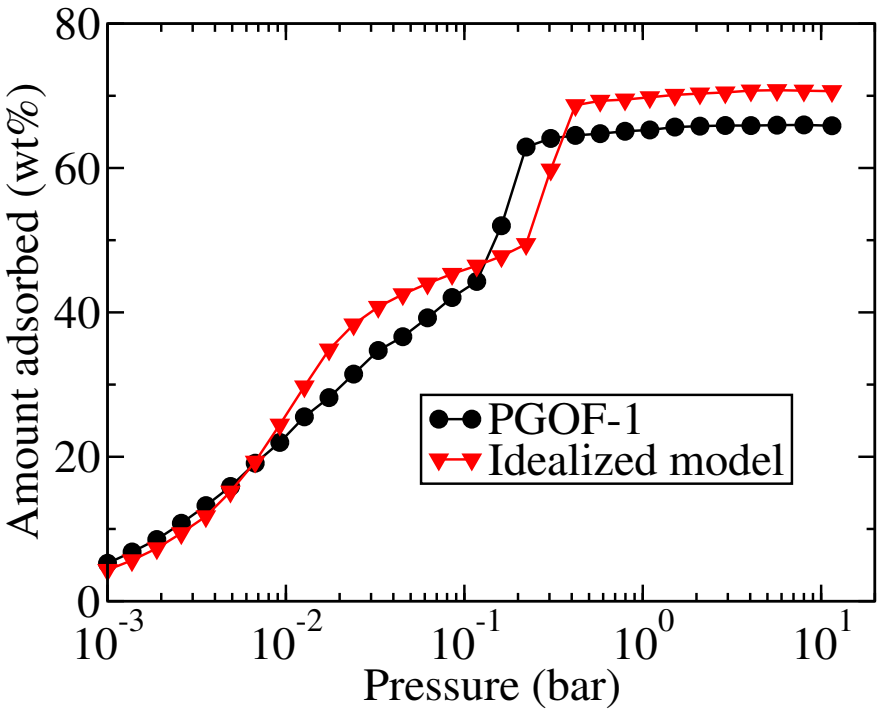

Figure 5: Adsorption isotherm of CO_2 at $T = 195$ K in PGOF-1 (circles) and in the idealized model (triangle).

At higher pressures, the situation is markedly different. The flat model results in a higher adsorption for both hydrogen and carbon dioxide. In the case of H_2, the amount adsorbed by the flat model is $\sim 14\%$ higher than the amount adsorbed by the realistic PGOF-1 model. In the case of CO_2, the amount adsorbed is as higher as $\sim 20\%$.

The origin of this difference cannot be attributed to the difference in the unit cell volume (as reported in Table 1).

In fact, the quantity used in the comparison – the weight percent of gas adsorbed – is intensive, thus not proportional to the mass of the unit cell. Indeed, an analysis based on the volumetric density of states,[49] corroborates this finding.

Taking hydrogen as a showcase, the average solid-fluid potential energy at the highest pressure investigated is comparable in the two models (-452 K for PGOF-1 and -448 K for flat model), as is the fluid-fluid potential energy per molecule (-52 K for PGOF-1 and -55 K for the flat model). Hence, the different amount of adsorbed molecules must be due to the fact that the fraction of the volume of the unit cell where the solid-fluid potential

energy results lower than ~ -450 K is larger for the flat model than for the realistic one.

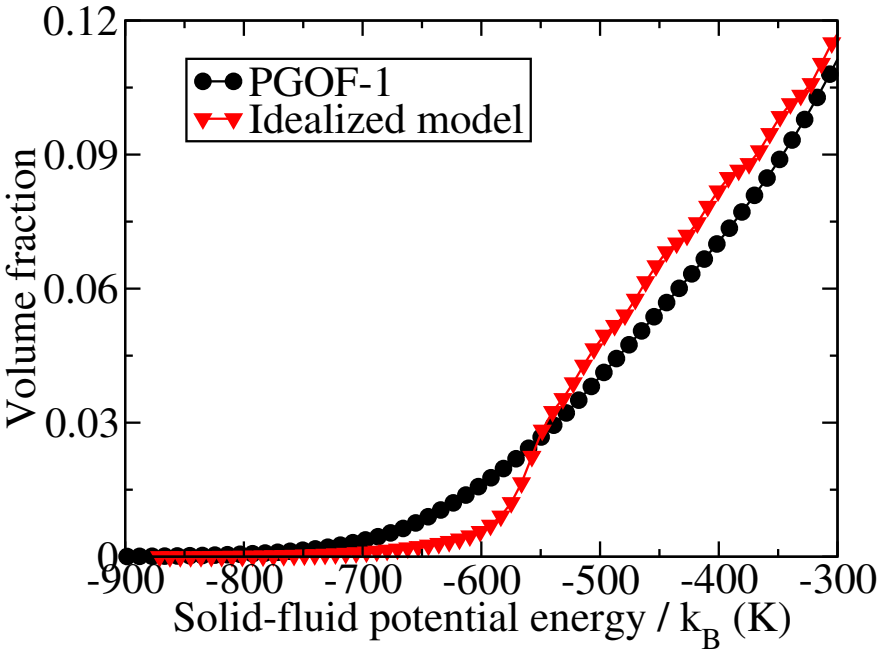

Figure 6: Fraction of unit-cell volume with solid-fluid energy less than a given value. Circles: PGOF-1, triangles: flat model.

The volume fraction having energy less than a certain amount is shown in Figure 6 for the realistic and the flat model. Again, one can notice that the realistic model has a larger volume available at the lowest energy (that is, around -600 K), which explains the larger adsorption at low pressure. When one considers the volume fraction where the energy is less then the measured solid-fluid potential at the highest pressure (that is, around -450 K), the trend is opposite. The flat model has a 15% larger volume fraction with solid-fluid interaction energy lower than -450 K and hence is capable of adsorbing more gas. One could then expect an adsorbed amount correspondingly higher, which is indeed in good agreement with the results of the GCMC simulations.

It is interesting to notice that at 10 bar of pressure, hydrogen is mostly found adsorbed close to the GO sheets, and has not yet occupied the whole available volume, as can be seen in the snapshots reported in Figure 7. A similar distribution is observed for CO_2 in the region around 20 mbar where the amount adsorbed in the flat model is considerably higher

than the amount adsorbed in the realistic one.

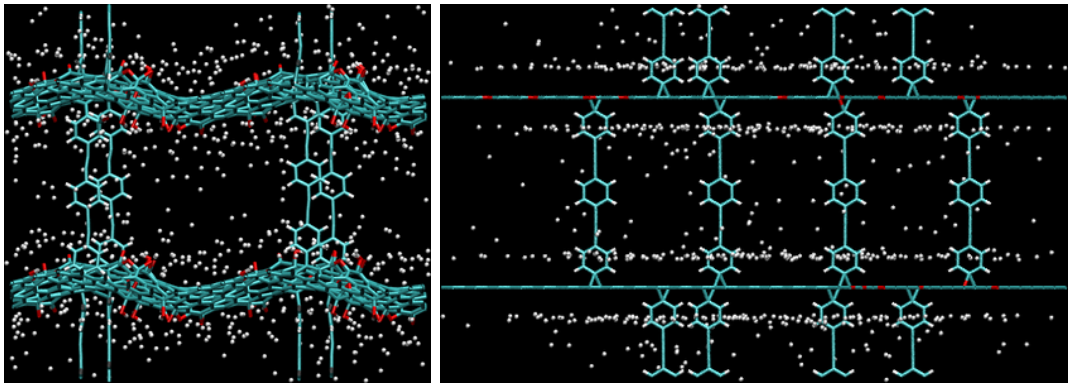

Figure 7: Simulation snapshots showing the typical distribution of hydrogen molecules (represented by white circles) adsorbed in PGOF-1 (left) and the flat model (right), at $T = 77$ K and $P = 10$ bar.

It is tempting to attribute also this different behavior to the corrugation of the graphene sheets. When compared to the perfectly flat GO sheets, the presence of concavities results in (small) regions with a smaller (more negative) interaction potential, hence a slightly larger adsorption at low external pressures. Conversely, close to the convexities of the realistic GO sheet, the solid-fluid potential energy is higher (less negative) than it would be in the perfectly flat situation. As a consequence of this corrugation, the volume fraction with favorable adsorption energy is smaller in the realistic sheet than in the perfectly flat one, resulting in a smaller amount of gas adsorbed.

These different adsorption could be used for instance to selectively release hydrogen as a result of a mechanical deformation.

CO_2/H_2 selectivity

We also investigated the selectivity of PGOFs, and the effect of the model on it, in the case of a binary mixture made by carbon dioxide and hydrogen. The selective adsorption of CO_2 from this mixture is an important step in the pre-combustion treatment of biogases.[50,59] In

the following, the selectivity of an adsorbent for a mixture of gases is defined by the ratio

$$S(b/a) = \frac{x_b/x_a}{y_b/y_a}, \tag{2}$$

where x_a denotes the molar fraction of the adsorbed species a and y_a the molar fraction of the same species in the bulk mixture in contact with the adsorbent (with a similar definition for the specie b). Values of $S(b/a)$ greater than one mean that the specie b is preferentially adsorbed with respect to the specie a.

Our results, reported in Fig. 8, show that the pressure dependence of the CO_2/H_2 selectivity at $T = 298$ K displays a similar trend for both the realistic and the idealized PGOF models. The selectivity remains constant up to roughly 1 bar of pressure, where it decreases and the increases again. The last points hint at a further decrease.

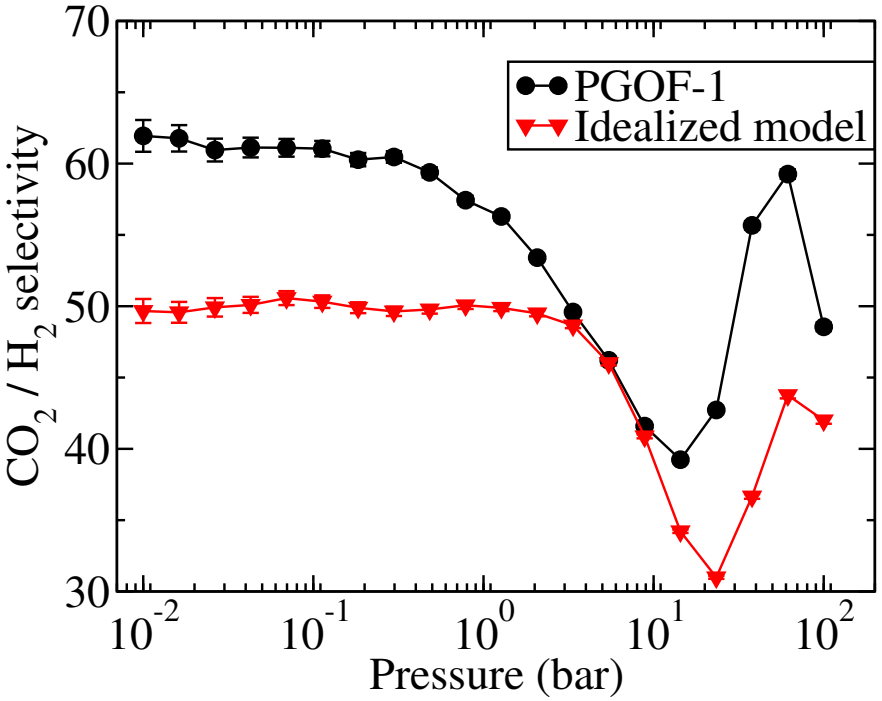

Figure 8: Pressure dependence of the CO_2/H_2 selectivity for an equimolar mixture at $T = 298$ K for PGOF-1 (circles) and its idealized model (triangles).

This trend, and the actual value of the selectivity between 50 and 60, are analogous to what has been observed, for the same mixture, in the case of adsorption in MOFs[60,61] or

in Zeolitic Imidazolate Frameworks.[62] The initial decrease of the selectivity with respect to the low-pressure limiting value is due to entropic effects dependent on the smaller size of the hydrogen molecule with respect to carbon dioxide. As the pressure is raised, however, the larger CO_2–CO_2 interaction favors the adsorption of carbon dioxide, resulting in an increase of the selectivity. At higher pressure still, entropy again favors hydrogen and the selectivity decreases again.

In the case of the selectivity, the principal difference between the realistic and idealized model is that the latter would predict a value of $S(CO_2/H_2)$ lower by roughly 15%.

Conclusions

In this paper, we presented computer simulation results of gas adsorption and separation in recently synthesized pillared graphene-oxide frameworks.

Using quantum chemical methods, we developed a realistic model of the framework, reproducing the observed oxygen density of the GO sheets, as well as all the various defects that oxidation produces in pristine graphene sheets. The optimized structures show that the presence of pillars results in a considerable corrugation of the GO sheets.

Computer simulation of hydrogen adsorption shows that the performance of these structures at cryogenic temperatures is comparable to that of Metal Organic Frameworks. When compared to the available experimental data, likely obtained with PGOFs having a different pillar density than the one we modeled, our results show that there is a large room for improvement in the amount of hydrogen that can be stored, possibly by a factor between two and three.

Conversely, computer simulation of carbon dioxide adsorption are comparable with the experimental data, although in our case pore condensation is observed in the highest pressure range. This difference might again be ascribed to the different density of pillars between the model and the actual samples.

Furthermore, we tested the reliability of the widely-used idealized models for these structures, built by simple juxtaposition of planar GO sheets and rigid linkers, without any further quantum mechanical optimization of the resulting structures.

The idealized models slightly underestimate the amount of gas adsorbed at low coverage, but significantly overestimate it (by $15-20\%$) in the region just before saturation, *i.e.*, when the gas molecules are adsorbed in the proximity of the GO sheets. This difference has been related to the corrugation of the GO planes.

Finally, we investigated the effect of modeling on the adsorptive separation of a CO_2/H_2 mixture. The values of the selectivity are comparable to the ones observed in MOFs, and display a similar pressure dependence. The idealized model underestimate $S(CO_2/H_2)$ by about 15%.

The results presented in this paper pave the way for a systematic investigation of the properties of PGOF as a function of the density of pillars and the specific moiety used as spacer. We showed how the results obtained with idealized models follow closely the results obtained with more realistic structures, generated using expensive ab-initio calculations, with the proviso that the measured properties (such as adsorbed amounts or selectivity) can be up to 15% different from the actual ones.

Acknowledgement

The research leading to these results has received funding from the European Union Seventh Framework Programme under grant agreement n. 604391 Graphene Flagship.

G.G. and S.T. acknowledge support by Istituto Nazionale di Fisica Nucleare through the "Supercalcolo" agreement with Fondazione Bruno Kessler. S.T. acknowledges economical support from the European Science Foundation under the INTELBIOMAT Exchange Grant "*Interdisciplinary Approaches to Functional Electronic and Biological Materials*" and the Bruno Kessler Foundation (FBK) for providing economical support through the "*research*

mobility scheme" under which this work has been accomplished. Furthermore, S.T. gratefully acknowledges the Institute of Advanced Studies in Bologna for the support given under his ISA research fellowship, and the high-performance computing service (PSMN) at the ENS de Lyon.

N.M.P. is supported by the European Research Council (ERC StG Ideas 2011 BIHSNAM n. 279985 on Bio-Inspired hierarchical super-nanomaterials, ERC PoC 2013-1 REPLICA2 n. 619448 on Large-area replication of biological anti-adhesive nanosurfaces, ERC PoC 2013-2 KNOTOUGH n. 632277 on Super-tough knotted fibres), by the European Commission under the Graphene Flagship (WP10 "Nanocomposites", n. 604391) and by the Provincia Autonoma di Trento ("Graphene Nanocomposites", n. S116/2012-242637 and delib. reg. n. 2266).

GCMC computer simulations were performed on the KORE computing cluster at Fondazione Bruno Kessler.

Supporting Information Available

Coordinate file for the structure shown in Figure 1 in XYZ format. The unit cell is orthorhombic with sides of length 44.0, 42.0, and 39.2 Å. This material is available free of charge via the Internet at http://pubs.acs.org/.

References

(1) Liao, L.; Lin, Y.-C.; Bao, M.; Cheng, R.; Bai, J.; Liu, Y.; Qu, Y.; Wang, K. L.; Huang, Y.; Duan, X. *Nature* **2010**, *467*, 305–308.

(2) Lin, Y.; Valdes-Garcia, A.; Han, S.-J.; Farmer, D. B.; Meric, I.; Sun, Y.; Wu, Y.; Dimitrakopoulos, C.; Grill, A.; Avouris, P. *Science* **2011**, *332*, 1294–1297.

(3) Cheng, R.; Bai, J.; Liao, L.; Zhou, H.; Chen, Y.; Liu, L.; Lin, Y.-C.; Jiang, S.; Huang, Y.; Duan, X. *Proc. Natl. Acad. Sci.* **2012**, *109*, 11588–11592.

(4) Taioli, S.; Umari, P.; De Souza, M. *Phys. Stat. Sol. (b)* **2009**, *246*, 2572–2576.

(5) Umari, P.; Petrenko, O.; Taioli, S.; De Souza, M. *J. Chem. Phys.* **2012**, *136*, 181101.

(6) Haberer, D.; Vyalikh, D. V.; Taioli, S.; Dora, B.; Farjam, M.; Fink, J.; Marchenko, D.; Pichler, T.; Ziegler, K.; Simonucci, S.; Dresselhaus, M. S.; Knupfer, M.; Büchner, B.; Grüneis, A. *Nano Letters* **2010**, *10*, 3360–3366.

(7) Haberer, D. et al. *Phys. Rev. B* **2011**, *83*, 165433.

(8) Henwood, D.; Carey, J. D. *Phys. Rev. B* **2007**, *75*, 245413.

(9) Ghosh, A.; Subrahmanyam, K. S.; Krishna, K. S.; Datta, S.; Govindaraj, A.; Pati, S. K.; Rao, C. N. R. *J. Phys. Chem. C* **2008**, *112*, 15704–15707.

(10) Ma, J.; Michaelides, A.; Alfè, D.; Schimka, L.; Kresse, G.; Wang, E. *Phys. Rev. B* **2011**, *84*, 033402.

(11) Tozzini, V.; Pellegrini, V. *Phys. Chem. Chem. Phys.* **2013**, *15*, 80–89.

(12) Dreyer, D. R.; Park, S.; Bielawski, C. W.; Ruoff, R. S. *Chem. Soc. Rev.* **2010**, *39*, 228–240.

(13) Joshi, R. K.; Carbone, P.; Wang, F. C.; Kravets, V. G.; Su, Y.; Grigorieva, I. V.; Wu, H. A.; Geim, A. K.; Nair, R. R. *Science* **2014**, *343*, 752–754.

(14) Cui, S.; Zhao, N.; Shi, C.; Feng, C.; He, C.; Li, J.; Liu, E. *J. Phys. Chem. C* **2014**, *118*, 839–844.

(15) Chan, Y.; Hill, J. M. *Nanotechnology* **2011**, *22*, 305403.

(16) Burress, J. W.; Gadipelli, S.; Ford, J.; Simmons, J. M.; Zhou, W.; Yildirim, T. *Angew. Chem. Int. Ed.* **2010**, *49*, 8902–8904.

(17) Srinivas, G.; Burress, J. W.; Ford, J.; Yildirim, T. *J. Mater. Chem.* **2011**, *21*, 11323–11329.

(18) Kumar, R.; Suresh, V. M.; Maji, T. K.; Rao, C. N. R. *Chem. Commun.* **2014**, *50*, 2015–2017.

(19) Tang, Q.; Zhou, Z.; Chen, Z. *Nanoscale* **2013**, *5*, 4541–4583.

(20) Li, H.; Eddaoudi, M.; O'Keefe, M.; Yaghi, O. *Nature* **1999**, *402*, 276–278.

(21) Babarao, R.; Jiang, J. *Langmuir* **2008**, *24*, 6270–6278.

(22) Wilmer, C. E.; Leaf, M.; Lee, C. Y.; Farha, O. K.; Hauser, B. G.; Hupp, J. T.; Snurr, R. Q. *Nature chemistry* **2012**, *4*, 83–89.

(23) Lin, L.-C.; Berger, A. H.; Martin, R. L.; Kim, J.; Swisher, J. A.; Jariwala, K.; Rycroft, C. H.; Bhown, A. S.; Deem, M. W.; Haranczyk, M. e. a. *Nature materials* **2012**, *11*, 633–641.

(24) Düren, T.; Sarkisov, L.; Yaghi, O.; Snurr, R. *Langmuir* **2004**, *20*, 2683–2689.

(25) Düren, T.; Bae, Y.-S.; Snurr, R. Q. *Chem. Soc. Rev.* **2009**, *38*, 1237–1247.

(26) Getman, R. B.; Bae, Y.-S.; Wilmer, C. E.; Snurr, R. Q. *Chem. Rev.* **2011**, *112*, 703–723.

(27) Nicolaï, A.; Zhu, P.; Sumpter, B. G.; Meunier, V. *J. Chem. Theory Comput.* **2013**, *9*, 4890–4900.

(28) Nicolaï, A.; Sumpter, B. G.; Meunier, V. *Phys. Chem. Chem. Phys.* **2014**, *16*, 8646–8654.

(29) Hummers, W.; Offeman, R. *J. Am. Chem. Soc.* **1958**, *80*, 1339–1339.

(30) Pei, S.; Cheng, H.-M. *Carbon* **2012**, *50*, 3210–3228.

(31) Bagri, A.; Mattevi, C.; Acik, M.; Chabal, Y. J.; Chhowalla, M.; Shenoy, V. B. *Nature chemistry* **2010**, *2*, 581–587.

(32) Kumar, P. V.; Bernardi, M.; Grossman, J. C. *ACS nano* **2013**, *7*, 1638–1645.

(33) Assfour, B.; Seifert, G. *Chem. Phys. Lett.* **2010**, *489*, 86–91.

(34) Assfour, B.; Leoni, S.; Seifert, G. *J. Phys. Chem. C* **2010**, *114*, 13381–13384.

(35) Zhou, W.; Wu, H.; Yildirim, T. *Chem. Phys. Lett.* **2010**, *499*, 103–107.

(36) Lukose, B.; Supronowicz, B.; Petkov, P.; Frenzel, J.; Kuc, A.; Seifert, G.; Vayssilov, G.; Heine, T. *Phys. Stat. Sol. (b)* **2012**, *249*, 335–342.

(37) Garberoglio, G.; Taioli, S. *Micropor. Mesopor. Mater.* **2012**, *163*, 215–220.

(38) Hanwell, M. D.; Curtis, D. E.; Lonie, D. C.; Vandermeersch, T.; Zurek, E.; Hutchison, G. R. *J. Cheminformatics* **2012**, *4*, 17.

(39) Halgren, T. *J. Comput. Chem.* **1996**, *17*, 490, See also the three subsequent papers in the same journal issue.

(40) Aradi, B.; Hourahine, B.; Frauenheim, T. *J. Phys. Chem. A* **2007**, *111*, 5678–5684, http://www.dftb-plus.info/.

(41) Kresse, G.; Hafner, J. *Phys. Rev. B* **1993**, *47*, 558.

(42) Alfè, D. *Comp. Phys. Comm.* **1999**, *118*, 31–33.

(43) Perdew, J. P.; Burke, K.; Ernzerhof, M. *Phys. Rev. Lett.* **1996**, *77*, 3865.

(44) Lukose, B.; Kuc, A.; Frenzel, J.; Heine, T. *Beilstein J. Nanotechnol.* **2010**, *1*, 60.

(45) Buch, V. *J. Chem. Phys.* **1994**, *100*, 7610–7629.

(46) Harris, J.; Yung, K. *J. Phys. Chem.* **1995**, *99*, 12021.

(47) Mayo, S.; Olafson, B.; Goddard III, W. *J. Phys. Chem.* **1990**, *94*, 8897.

(48) Rappé, A.; Casewit, C.; Colwell, K.; Goddard III, W.; Skiff, W. *J. Am. Chem. Soc.* **1992**, *114*, 10024.

(49) Garberoglio, G.; Skoulidas, A.; Johnson, J. *J. Phys. Chem. B* **2005**, *109*, 13094–13103.

(50) Sumida, K.; Rogow, D. L.; Mason, J. A.; McDonald, T. M.; Bloch, E. D.; Herm, Z. R.; Bae, T.-H.; Long, J. R. *Chem. Rev.* **2011**, *112*, 724–781.

(51) Feynman, R.; Hibbs, A. *Quantum Mechanics and Path-Integrals*; McGraw-Hill, 1965.

(52) Wang, Q.; Johnson, J. K.; Broughton, J. Q. *J. Chem. Phys.* **1997**, *107*, 5108.

(53) Garberoglio, G. *J. Chem. Phys.* **2008**, *128*, 134109.

(54) Garberoglio, G.; Johnson, J. *ACS Nano* **2010**, *4*, 1703.

(55) Garberoglio, G. *Chem. Phys. Lett.* **2012**, *525-526*, 19.

(56) Rouquerol, J.; Rouquerol, F.; Llewellyn, P.; Maurin, G.; Sing, K. S. *Adsorption by powders and porous solids: principles, methodology and applications*; Academic press, 2013.

(57) Garberoglio, G. *Langmuir* **2007**, *23*, 12154–12158.

(58) Walton, K. S.; Millward, A. R.; Dubbeldam, D.; Frost, H.; Low, J. J.; Yaghi, O. M.; Snurr, R. Q. *J. Am. Chem. Soc.* **2008**, *130*, 406–407.

(59) Li, J.-R.; Ma, Y.; McCarthy, M. C.; Sculley, J.; Yu, J.; Jeong, H.-K.; Balbuena, P. B.; Zhou, H.-C. *Coord. Chem. Rev.* **2011**, *255*, 1791–1823.

(60) Yang, Q.; Zhong, C. *J. Phys. Chem. B* **2006**, *110*, 17776–17783.

(61) Yang, Q.; Xu, Q.; Liu, B.; Zhong, C.; Berend, S. *Chin. J. Chem. Eng.* **2009**, *17*, 781–790.

(62) Battisti, A.; Taioli, S.; Garberoglio, G. *Micropor. Mesopor. Mater.* **2011**, *143*, 46.